ACS APPLIED MATERIALS & INTERFACES

Applications of Polymer, Composite, and Coating Materials

Carbon-GO Composites with Preferential Water versus Ethanol Uptakes

lizhi Guan, Julian Patiño, Carlos Cuadrado-Collados, Aitana Tamayo, Maria C. Gutiérrez, María Luisa Ferrer, Joaquin Silvestre-Albero, and Francisco del Monte

ACS Appl. Mater. Interfaces, **Just Accepted Manuscript** • DOI: 10.1021/acsami.9b02745 • Publication Date (Web): 14 Jun 2019

is published by the American Chemical Society. 1155 Sixteenth Street N.W., Washington, DC 20036

Carbon-GO Composites with Preferential Water versus Ethanol Uptakes

Li Zhi Guan,[a] Julian Patiño,[a] Carlos Cuadrado-Collados,[b] Aitana Tamayo,[c] María C. Gutiérrez,[a] M. Luisa Ferrer,[a] Joaquín Silvestre-Albero,[b] Francisco del Monte*, [a]

[a] *Materials Science Factory, Instituto de Ciencia de Materiales de Madrid-ICMM, Consejo Superior de Investigaciones Científicas-CSIC, Campus de Cantoblanco, 28049, Madrid, Spain;* [b] *Laboratorio de Materiales Avanzados, Departamento de Química Inorgánica-Instituto Universitario de Materiales, Universidad de Alicante, Ctra. San Vicente-Alicante s/n, E-03690 San Vicente del Raspeig, Spain;* [c] *Instituto de Cerámica y Vidrio-ICV, Consejo Superior de Investigaciones Científicas-CSIC, Campus de Cantoblanco, 28049, Madrid, Spain*

Abstract

The elimination of tiny amounts of water from alcohols is by no means a trivial issue in many practical applications like, for instance, the dehumidification of biocombustibles. The use of carbonaceous materials as sorbents has been far less explored than that of other materials because their hydrophobic character has typically limited their water uptake. Herein, we designed a synthetic process based on the use of eutectic mixtures that allowed the homogeneous dispersion of graphene oxide (GO) in the liquid containing the carbon precursor – e.g., furfuryl alcohol. Thus, after polymerization and a subsequent carbonization process, we were able to obtain porous carbon-GO composites where the combination of pore diameter and surface area hydrophilicity provided a remarkable capacity for water uptake but extremely low methanol and ethanol uptakes along the entire range of relative pressures evaluated in this work. Both the neat water uptake and the uptake difference between water and both methanol and ethanol of our carbon-GO composites were similar or eventually better that uptakes previously reported for other materials also exhibiting preferential water-to-alcohol adsorption – e.g., porous coordination polymers, MOFs, polyoxometalates, and covalent 2D nanosheets embedded in a polymer matrix. Moreover, water versus alcohol uptakes were particularly remarkable at low partial pressures in our carbon-GO composites.

Introduction

The use of porous carbons – with high specific surface area (SSA), pores diameter matching the size of interest and "a la carte" pore surface functionalization – has attracted great interest in number of applications, from electrodes in energy storage devices to substrates for gas adsorption and separation. Porous carbons with a three dimensional (3D) hierarchical porous structure (combining micro-, meso- and/or macropores) are particularly interesting because of the combination of mass transport properties provided by large pores – e.g., large meso- and macropores – and high surface areas provided by small pores – e.g., small meso- and micropores. In this regard, a number of synthetic routes have been explored by using different carbonaceous precursors and either template-based or template-free approaches to modulate the porous texture of the resulting carbon structures.[1-3] Recent efforts have also been focused on the preparation of porous carbon composites containing graphitic carbon entities – e.g., carbon nanotubes,[4] nanohorns,[5] or graphene oxide (GO),[6] among the most remarkable cases. The main challenge in these cases was to obtain a homogeneous dispersion of these entities throughout the 3D hierarchical porous structure to guarantee the proper and uniform function of the resulting composite.

Among the above mentioned applications, the use of porous carbons and carbon composites as sorbents for gas adsorption and gas separation purposes has been widely explored because the combination of high performance, good structural stability and low cost make them quite attractive as compared to other sorbents. For instance, number of porous carbons and carbon composites has exhibited high adsorption capabilities for not only gases like N_2 or CO_2[7-11] but also vapours of water, alcohols, etc.[12-16] Nonetheless, it is worth noting that whereas carbon and carbon composites were highly effective for gas separation, the use of carbon materials for separation of water, methanol, and ethanol has been far less explored than for other sorbents. It should be noted that in comparison to traditional distillation methods, selective adsorption of water/methanol and/or water/ethanol could provide an energetically efficient and sustainable way to biofuel production. Nonetheless, it is by no means trivial finding suitable porous materials as sorbents given the chemical similarities among these three solvents. For instance, porous coordination polymers (PCPs) and iso-reticular metal–organic frameworks (MOFs) – i.e., with tunable pore sizes and shapes, and with specific surface chemical properties – as well as polyoxometalates had proved highly effective in the separation of methanol and water from a water−methanol−ethanol mixture thus favouring the use of bioethanol as an alternative energy source.[17-24] More recently, nanofibrous membranes containing a GO barrier layer have also been used for ethanol dehydration[25, 26] whereas the use of carbonaceous porous solids for these purposes have

basically been limited to those derived from cycloparaphenylene.[27] This limited number of studies using carbonaceous materials should most likely be attributed to some intrinsic features of the carbon itself such as its major hydrophobic nature conferred by pure aromatic layers.[28] Modifying the surface chemistry to infer certain hydrophilicity while tuning pore diameters for discrimination between water and alcohols – i.e., according to their respective kinetic diameters – are the challenges to circumvent the problem that nowadays limits the use of carbonaceous materials in this interesting field.

Our group has recently reported on the preparation of carbon materials and carbon composites with hierarchical porous structures through a quite versatile synthetic approach.[29] In particular, we used eutectic mixtures (described as either deep eutectic solvents – DESs – by Abbott and coworkers,[30-33] or low-transition-temperature mixtures – LTTMs – by Kroon and coworkers[34]) composed of resorcinol (Re) and choline chloride (ChCl) so that Re polycondensated with formaldehyde to, after carbonization, obtain monolithic carbons built of highly cross-linked clusters that aggregated and assembled into a stiff and interconnected structure.[35] The high conversion in which Re becomes the material itself and the feasible recovery of ChCl – and hence, its reuse in subsequent reactions – make DES-assisted syntheses very efficient in terms of reagent economy.[9, 36] The use of DESs was particularly interesting to prepare carbon materials doped with different heteroatoms and tailored porous structures[7-9, 37-42] as well as carbon composites with carbon nanotubes.[43, 44]

Herein, we explored the preparation of carbon composites with GO for separation of water, methanol, and ethanol. For this purpose, GO flakes were homogeneously dispersed in a DES obtained by mixing phosphoric acid (PA), ethylamine hydrochloride (EA) and glycerol (Gly) in a 1:2:1 molar ratio. Furfuryl alcohol (FA) was added to the homogeneous dispersion of GO in DES resulting after lyophilisation to promote FA polycondensation – i.e., catalyzed by the PA-containing DES. The degree of condensation of the polymers resulting after polycondensation was studied by ^{13}C NMR and FTIR spectroscopies. Subsequent carbonization resulted in the formation of carbon-GO composites in the form of porous monoliths. The morphology of the resulting materials was studied by scanning electron microscopy (SEM). Carbon-GO composite exhibited capabilities for both adsorption of water vapours and separation of water from ethanol in the vapour phase that were in range to those of the most remarkable sorbents mentioned above – e.g., MOFs and GO-based membranes.

Experimental

Preparation of Deep Eutectic Solvent (DES):

DES was obtained as described elsewhere[44] but using phosphoric acid (85% in water, PA), ethylamine hydrochloride (EA) and glycerol (Gly) in a 1:2:1 molar ratio and a thermal treatment of 120 °C over 30 min.

Preparation of graphene oxide (GO):

Graphene oxide (GO) was obtained from graphite following Hummers–Offeman method[45] and as described in detail elsewhere.[46]

Preparation of carbon-GO composites:

In a typical synthesis, 1 g of DES was mixed with 1 mL of the above-described GO dispersion by mechanical stirring. The resulting mixture was frozen and lyophilized in order to eliminate water. Carbon-GO composites were prepared as described in detail elsewhere.[43] Briefly, 0.2 g of furfuryl alcohol (FA, 99.8 wt%) were added to the dispersion of GO in DES obtained after lyophilisation. FA polycondensation was achieved as described elsewhere.[43] The resulting polymeric resins were thermally treated for 4 h at 800 or 950 °C (heating ramp was 1.0 °C min^{-1}) under nitrogen atmosphere. Carbons without GO were also prepared as controls. For this purpose, 1 g of DES was mixed with 0.2 g of FA and vortexed for 2 min. Polycondensation and subsequent carbonization were performed as described above.

Characterization of DES:

DES was studied by ^{1}H NMR spectroscopy as described elsewhere.[35] Thermogravimetric analyses (TGA) were performed with a SDT-Q600 from TA instruments, under a nitrogen atmosphere and using a heating rate of 5 °C min^{-1}. Differential scanning calorimetry (DSC) was performed with a TA Instruments Model DSC Q-100 system, under a nitrogen atmosphere. The samples were run in an aluminium pan in a sealed furnace, stabilized for 10 min at 20 °C, and then cooled to -90 °C before heating at rates of 5 °C min^{-1}. Water content of the as-prepared DES, the DES after lyophilisation, and the dispersion of GO in DES after lyophilisation were determined by Karl-Fisher method using a Metrohm Titrando 888.

Characterization of the polymeric resin resulting from FA polycondensation:

FTIR spectra were recorded as described elsewhere.[44] ^{13}C and ^{31}P solid-state NMR spectroscopic studies were carried out in a Bruker Advance 400 MHz Wide Bore (9.39 T) spectrometer as described elsewhere,[44] except for the pulse width and the number of scans – e.g., 6.2 μs and 1024 scans, in this case.

Characterization of GO and carbon-GO composite:

Raman spectra of GO and the carbon-GO composite were recorded as described elsewhere.[44] The ^{31}P NMR spectrum of the carbon-GO composite was acquired as described previously,[44] except for using a pulse width of 4.0 μs, a recycle delay of 20 s, an acquisition time of 44 ms. a total of 228 scans and a field strength of 55 kHz. The morphology of the carbon-GO composite

was also studied as described previously.[44] The complex Young's modulus of the carbon-GO composite was measured at 1 Hz in a triple-point bending configuration by using a DMA 7e dynamic mechanic analyzer (Perkin-Elmer). The direct current conductivity (σ_{DC}) of the carbon-GO composite was measured by using a digital multimeter Fluke 8840A in a four-probe configuration, as described in detail elsewhere.[43] XRD spectra of carbon-GO composites were recorded in a Bruker D8 Advance difractometer using the CuKα radiation (0.02° step size and 1.0 s counting time). Total reflection X-ray fluorescence (TXRF) analysis of the carbon-GO composite was carried out on a S2 PicoFox spectrometer. X-Ray Photoelectron spectroscopy (XPS) surface analysis of GO and the carbon-GO composite was performed as described in detail elsewhere.[44] Elemental chemical analysis (ECA) of the carbon-GO composite was performed in an LECO Elemental Analyzer CHNS-932. The nitrogen adsorption/desorption isotherm of the carbon-GO composite was carried out at −196 °C in an ASAP 2020 from Micromeritics on samples previously outgassed under dynamic vacuum (ca. 10^{-5} torr) at 200 °C for 12 hours. As described in detail elsewhere,[40] we applied the Brunauer-Emmett-Teller (BET) theory and the Barrett-Joyner-Halenda (BJH) method (based on the desorption branches of the isotherms) to calculate the specific surface areas and pore-size distributions, respectively. The analyzer was equipped with a pressure transducer of capacity 1000 mmHg (accuracy within 0.15 % of reading). Immersion calorimetry measurements of carbon-GO composites were performed in a C80D calorimeter (SETARAM) working at 30 °C as depicted in Fig. S1 and described in detail elsewhere.[47] A complete description of the experimental setup can be found in the literature.[48] Water and alcohol adsorption measurements of carbon-GO composites were performed in a vapor adsorption equipment designed and constructed by the LMA group and now commercialized by Quantachrome as Vstar. Samples were outgassed under ultrahigh-vacuum at 200 °C for 12 h before calorimetric and vapor adsorption measurements.

Results and Discussion

The eutectic mixture of PA, EA and Gly – e.g., $PAEAGly_{DES}$ – was obtained by physical mixing of the individual components in a 1:2:1 molar ratio and the subsequent thermal treatment at 120 °C over 30 min. The molten mixture remained in the liquid phase when returned to room temperature. Karl Fischer titration revealed the presence of ca. 1.1 mol of water per mol of DES, most likely coming from the use of an aqueous PA solution for $PAEAGly_{DES}$ preparation. In these conditions, one should consider $PAEAGly_{DES}$ as a quaternary DES composed of PA, EA, Gly, and water more than a ternary one just composed to PA, EA and Gly.[49] Submission of $PAEAGly_{DES}$ to lyophilisation resulted in a significant decrease of the water content to less than

0.4 mol per mol of DES. The role played by water as one of the DES components was corroborated by DSC. DSC scans of $PAEAGly_{DES}$ before lyophilisation revealed the presence of a melting at a temperature (T_m) of ca. 20 °C. This T_m increased up to 36 °C after lyophilisation and a glass transition temperature (T_g) at ca. –80 °C also appeared (Fig. 1). ^{1}H NMR spectroscopy confirmed the reduced water content in lyophilised $PAEAGly_{DES}$ – i.e., the sum of exchangeable protons integrated at the peak at ca. 7.4 ppm was 12 H, this is, 3H coming from 1 equivalent of PA, 6H coming from 2 equivalent of EA and 3H coming from 1 equivalent of Gly. The upfield chemical shift experienced by EA peaks in the lyophilized $PAEAGly_{DES}$ is the typical signature of compounds acting as HBAs in eutectic mixtures,[50-52] thus corroborating the formation of H-bond complexes among PA, EA and Gly (Fig. S2 and Table S1). This result disregarded the hypothetical case where one of the precursors is just dissolved in the respective binary DES because, if so, the chemical shifts of this dissolved precursor would be closer to those of its individual components.[41]

Meanwhile, GO flakes were prepared by chemical oxidation of commercial graphite powder using a modified Hummers and Offeman method.[45] The lateral size of the resulting GO flakes was about 2.5 μm according to TEM micrographs (Fig. 2a and 2b). Chemical characterization of the as-prepared GO powder was performed by XPS and XRD (Fig. 2c and 2d). C1s peak was deconvoluted in three contributions, one at a binding energy of 284.8 eV assigned to C–C, C=C, and C–H bonds, a second one at a binding energy of 286.2 eV assigned to C–OH bonds, and third one at 288.2 eV assigned to C=O bonds (both carbonyl and carboxyl groups).[53, 54] The contribution of neither hydroxyl and epoxide nor carbonyl and carboxyl functional groups was separated in the deconvoluted C(1s). In the former case, both groups exhibited similar binding energies[53] whereas, in the latter one, overlapping of the very-low-intensity peak of carboxyl groups with the high-intensity peak of carbonyl ones made also difficult a reliable deconvolution. Meanwhile, a broad peak at ca. 11° (*d*-spacing ca. 8.03 Å) typical of hydrophilic and oxidized GO flakes was observed by XRD (Fig. 2d).[55]

We also used Raman spectroscopy to obtain information about the structural features of our GO (Fig. 3 and Table S2). As described elsewhere,[56] "D band refers to the structural disorder related to the sp^3-hybridized carbon bonds such as hydroxyl and/or epoxide bonds, and the G band comes from the sp^2 bond stretching of carbon atoms". The I_D/I_G ratio was ca. 0.705 in our case (Table S2) in agreement with the presence of oxygenated groups previously revealed by XPS spectra (Fig. 2c). Further information of the oxidation degree can be obtained from both the wavenumber and full width half maximum (FWHM) of G band. In our case, the position of G band – located at ca. 1592 cm^{-1} – and its FWHM – of ca. 96 cm^{-1} – indicated a high oxidation level (Table S2).[57] Besides G and D bands, there are two important peaks with

weaker intensity called 2D (second order of the D-peak) and D+G located at ca. 2722 and 2935 cm^{-1}, respectively. The I_{2D}/I_G ratio was calculated from the intensity of 2D and G bands. This ratio allows estimating the number of layers of GO flakes – i.e., above 1.6, ca. 0.8, ca. 0.30 and ca. 0.07, for single-, double-, triple- and multi-layer (>4), respectively. In our case, we found a I_{2D}/I_G ratio of ca. 0.196, so the averaged number of layers of our GO flakes was above 3 (Table S2).[56, 57]

The dispersion of GO flakes in $PAEAGly_{DES}$ was achieved by mixing an aqueous GO dispersion with $PAEAGly_{DES}$ and, then, submitting this liquid binary dispersion to lyophilisation for water elimination (Fig. 4a). Karl Fischer titration revealed some remaining water – ca. 1.2 mol of water per mol of DES – after lyophilisation. DSC scans of $PAEAGly_{DES}$ containing GO revealed the presence of a melting at T_m of ca. 16 °C (Fig. 1), this is similar to the T_m observed for $PAEAGly_{DES}$ before lyophilisation. Actually, the water content in $PAEAGly_{DES}$ containing GO was similar to that found in $PAEAGly_{DES}$ before lyophilisation – ca. 1.2 and 1.1 mol of water per mol of DES, respectively. This high water content in $PAEAGly_{DES}$ containing GO even after lyophilisation should most likely be ascribed to the surface functionalization of our GO and its capability to adsorb water. The hydrophilic features of our GO were actually corroborated by the mass loss observed in the TGA at temperatures below 100 °C and ascribed to moisture and adsorbed water (Fig. S3).

FA polycondensation was promoted as described in the experimental part and in some of our previous works.[43] Both methylene (by condensation of a hydroxyl group of one furan with the C5-hydrogen of another) and methylene ether bridges (by condensation between the hydroxyl groups of two different furans) are formed by acid catalysed condensation, being the former more abundant than the latter according to the polymerization pathways proposed elsewhere (Fig. S4).[44, 58] FTIR and solid ^{13}C NMR spectroscopies were used to study the relative abundance of methylene and methylene ether groups and thus determine whether the use of a protic DES (rather than acidic water as solvent) had any influence on polycondensation (Fig. 5). Thus, the signals at 744, 1149, 1560 and 3106 cm^{-1} in the FTIR spectrum were attributed to furan rings while signals at 788 and 1560 cm^{-1} corresponded to bending out of plane of CH_2 linkage and to the stretching of -C=C- groups in 2-5 disubstituted furanic rings, respectively (Fig. 5a). Bands assigned to methylene (CH_2 groups) were also observed at ca. 2917 and 1421 cm^{-1} whereas the presence of bands assigned to methylene ether groups (C-O benzyl ether groups, at ca. 1230 and 1100 cm^{-1}) was unclear (Fig. 5a). The solid ^{13}C NMR spectrum provided useful information with regards to this issue. Thus, the spectrum depicted in Fig. 5b was the typical for FA condensed via methylene bridges with peaks at ca. 27 ppm (assigned to methylene bridges), 108 ppm (assigned to C3 in FA condensed via methylene bridges) and 151

ppm (assigned to C2 in FA condensed via methylene bridges). The low intensity of the peak at 110 ppm (actually, appearing as a shoulder of that at 108 ppm) assigned to C3 in FA condensed via methylene ether bridges and the absence of the peak at 64 ppm assigned to methylene ether bridges further confirmed that FA condensation occurred via methylene (rather than via methylene ether) bridges.[58] Solid ^{13}C NMR spectroscopy also revealed that cross-linking of linear FA oligomers occurred by the formation of -CH_2- linkages between both the methylene groups of adjacent FA oligomers (peak at ca. 39 ppm) and the C3 of FA (Fig. 5b).

Carbonization of FA resins was accomplished at 800 °C in N_2 atmosphere with remarkable carbon conversions of about 60 %, this is, in range to those obtained for bare FA resins and CNT-based FA resins.[43] The resulting carbon-GO composites were obtained in the form of monoliths exhibiting an excellent mechanical stability (Fig. 4b) thanks to the continuous porous network structure built of colloidal clusters, as revealed by SEM and TEM (Fig. 6a, 6b and 6c). It is worth noting that thanks to this continuous structure, the carbon-GO composite also exhibited a remarkable electrical conductivity (σ_{DC}) of ca. 2.7 S cm^{-1}. SEM and TEM micrographs also revealed the presence of thin layers connecting colloids that resembled GO – or, considering the thermal stability of GO, some evolved GO – that were not observed in carbons without GO (Fig. S5). Thermal stability of GO is actually an issue – i.e., previous reports have described mass losses of ca. 50 % – so its presence in the resulting carbon-GO composites was investigated by TGA (Fig. S3).[59] For this purpose, we studied the GO used for preparation of carbon-GO composites, the FA resin with GO used for preparation of carbon-GO composites, and a FA resin identical to this latter one but without GO. As mentioned above, GO exhibited a significant mass loss below 100 °C due to the loss of moisture and adsorbed water while the mass loss in the temperature range of 150–300 °C was ascribed to the pyrolysis of labile oxygen-containing functional groups, yielding CO and CO_2.[59] In agreement with previous works, our GO exhibited a mass loss of up to 77 % at 800 °C[60] so one might question whether the presence of GO was significant in the carbon-GO composites. Nonetheless, it is worth noting that mass losses ranging from 77 to 71 % were also observed at 800 °C in both FA resins whereas the carbonization process used for achieving carbons and carbon-GO composites from FA resins provided carbon conversion of ca. 60 %. This decrease in the mass loss – e.g., 40 % in the carbonization process versus 77-71 % in TGA – should be ascribed to differences in the heating ramp – e.g., 1.0 °C min^{-1} in the carbonization process versus 5.0 °C min^{-1} in TGA – that, most likely, also played a role in the mass loss of GO. Actually, the differences in mass loss between carbons and carbon-GO composites observed in the TGA allowed estimating a GO content of ca. 6 wt% in carbon-GO composites.

The nature of GO incorporated in the resulting carbons was also investigated by Raman spectroscopy. Thus, Fig. 3 shows the Raman spectra of GO, the carbon-GO composite and an equivalent carbon without GO, all obtained by carbonization at 800 °C using a heating ramp of 1.0 °C min^{-1}. In compare to the Raman spectrum of GO, carbonization modified the chemical features of GO just slightly, evolving the I_D/I_G ratio from ca. 0.705 to ca. 0.720, and the position and FWHM of G band from 1592 to 1590 cm^{-1} and from 96 to 90 cm^{-1}, respectively (Fig. 3 and Table S2). Interestingly, the I_D/I_G ratio of the carbon without GO was 0.932 whereas that of the carbon-GO composite was 0.827, this is, in between those of the carbonized GO and the carbon without GO thus revealing how the chemical features of the carbon-GO composite corresponded to a combination of the chemical features of GO and carbon. This was also the case for the carbon-GO composite and an equivalent carbon without GO obtained by carbonization at 950 °C (Fig. S6). The XRD pattern displayed the typical broad peak of amorphous carbons (Fig. 6d).

XPS was also utilized to study the composition and the graphitic content of carbon-GO composites obtained by carbonization at 800 °C. The fitting parameters of the asymmetric peak were chosen so as to obtain the best fit (Fig. 6f and Table S3). Thus, the consistent fitting of the C1s level needed of a sum of four peaks. The peak at lowest binding energy – e.g., 284.8 eV – was ascribed to graphitic sp^2 configurations.[61-63] The peaks at 286.3, 287.6 and 289.4 eV were ascribed to, respectively, hydroxyl, carbonyl and carboxyl groups, thus confirming the presence of oxygen-containing groups attached to the carbon backbone. Moreover, the N1s deconvolution of the XPS spectrum provided three peaks ascribed to the following nitrogen functionalities of carbon-GO composites; pyridinic-N at 398.5 eV, pyrrolic-N at 400.3 eV, and quaternary-N at 402.0.[64, 65]

As revealed by EDX-SEM, ECA, TXRF, and XPS, the presence of EA and PA during carbonization introduced nitrogen and phosphorus functionalities, respectively, on the porous surface of the resulting carbons. Nitrogen and phosphorus contents were respectively ca. 3.6 and 14.5 wt% according to EDX and ca. 2.3 and 7.9 wt% according to XPS (Tables S3 and S4). The phosphorus content obtained from TXRF agreed with that obtained from EDX whereas ECA provided a nitrogen content in between those mentioned above for EDX and XPS (Table S4). Solid-state ^{31}P NMR spectroscopy and XPS confirmed this P-functionality was mainly in the form of phosphate moieties (Fig. 6e).

We also attempted measuring the N_2 isotherms but adsorption was negligible (Fig. S7). One may wonder whether the resulting carbon-GO composites were not porous. However, the occurrence of negligible N_2 adsorption is somehow common in samples with narrow micropores so that gas entrance is restricted at cryogenic temperatures due to diffusional

restrictions.[8, 9, 39, 66-68] In these cases where the determination of the textural properties by N_2 adsorption isotherms at −196 °C is not possible, immersion calorimetry offers a reliable alternative to disregard whether a certain sorbent is porous or not.[69, 70] Immersion calorimetry provides a measurement of the 'heat' evolved when a solid is immersed into a non-reacting liquid because of the formation of an adsorbed layer of the liquid's molecules on the solid's surface.[48] The experimental conditions differ from those of N_2 adsorption isotherms – uses liquids and the experiment is carried out at 30 °C, see experimental part – but it may provide an indirect measurement of the surface area and pore size distribution of microporous sorbents in the absence of specific interactions at the solid−liquid interface and selecting liquids with molecular dimensions in range to the pore diameter. In our case, the liquid of choice was dichloromethane (DCM) because of its small kinetic diameter – e.g., ca. 0.33 nm, this is, slightly below that of N_2 (0.36 nm). Then, we performed immersion calorimetry in carbon-GO composites obtained using both 800 and 950 °C as the carbonization temperature. It is worth noting that negligible changes were observed in the XRD of both samples (Fig. 6 and Fig. S8). The surface area estimated from the heats of immersion found for DCM – after calibration with the appropriate reference (e.g., a nonporous V3G carbon) – was 165 and 265 $m^2\ g^{-1}$, respectively. These measurements confirmed that the absence of N_2 adsorption was reflecting an erroneous lack of porosity because of the kinetic restrictions experienced by this particular gas at this particular temperature to reach the most inner porosity of our samples. Moreover, one could anticipate the occurrence of limited adsorptions – i.e., because of narrow constrictions – of molecules with kinetic diameters around 0.36 nm and above.

Hierarchical pore architectures prepared from and/or entrapping different sorts of two-dimensional (2D) nanosheets surface decorated with hydrophilic functionalities – e.g., GO – proved highly effective for water uptake and water/alcohol separation.[71-74] Based on this, we investigated the performance of porous carbon-GO composites for water uptake and water separation from ethanol and methanol – i.e., alcohol dehydration. In particular, we focussed on carbon-GO composites obtained using both 800 and 950 °C as the carbonization temperature. As shown in Fig. 7 and Fig. S9, significant differences can be observed in the adsorption isotherms of these three molecules. Water was gradually adsorbed, more so in the low-pressure region – e.g., up to relative pressures of ca. 0.3-0.4 – and less afterwards, reaching final uptakes of ca. 10 and 12 mmol g^{-1} of sorbent for the carbon-GO composites obtained at 800 and 950 °C, respectively (Fig. 7 and Fig. S9). The isotherm shape actually resembled that of activated carbons with ultramicropores.[75] Large water uptakes in the low-pressure range have been previously observed in other hydrophilic sorbents, thus revealing the hydrophilic nature of our carbon-GO composite. It is widely accepted that hydrogen

bonding interactions play a significant role in the adsorption of water vapour onto the hydrophilic surface of porous materials.[17, 20, 24] In general, oxygen-containing groups are able to act as primary adsorption centres due to the formation of hydrogen bonds with adsorbing water molecules.[20, 76] When water molecules attach to the centre, it will form a secondary adsorption site on which additional water molecules can be further adsorbed.[20, 77] Contrary to water, methanol was not preferentially adsorbed in the low-pressure region, exhibiting the isotherm a clear step at relative pressures ranging from 0.1 to 0.4 (Fig. 7 and Fig. S9) that resembled the gate-open adsorption isotherms described in previous works.[17, 20] Actually, equilibration times experienced a significant increase along the relative pressures of the step (see lower panel in Fig. 7), thus suggesting some important kinetic restrictions in this relative pressure range. Total methanol uptake was below that of water – e.g., ca. 3.6 mmol g^{-1} of sorbent for the carbon-GO composites obtained at 800 °C and ca. 4.6 mmol g^{-1} of sorbent for the carbon-GO composites obtained at 950 °C. Finally, ethanol uptake was very small – e.g., ca. 1.3 mmol g^{-1} of sorbent for the carbon-GO composites obtained at 800 °C and ca. 2.0 mmol g^{-1} of sorbent for the carbon-GO composites obtained at 950 °C – with a steady increase of adsorption over the whole range of relative pressures. Interestingly, GO played a critical role in the adsorption features of carbon-GO composites as demonstrated by the adsorption isotherms of carbons without GO where most of the remarkable features described above were depleted or even missed – for instance, the preferred water versus alcohol uptake at low partial pressures (Fig. S10).

Considering the differences in molecular size for water, methanol and ethanol, we also found of interest providing adsorption data in $cm^3\ g^{-1}$ (Fig. S11). In this case, adsorption isotherms kept revealing a high capacity for water uptake – more so for the carbon-GO composites obtained at 950 °C – and a preferred uptake of water over alcohols – for methanol at $P/P_0 = 0.1$ and in the whole range of relative pressures for ethanol, being more accused for the carbon-GO composites obtained at 800 °C. The occurrence of such a preferred uptake of water even upon the representation of adsorption data in $cm^3\ g^{-1}$ indicated how kinetic restrictions – more so than thermodynamical aspects – played a role in the limited adsorption experienced by methanol and ethanol in our carbon-GO composites.

Table 1 including data in both mmol g^{-1} and $cm^3\ g^{-1}$ obtained for the most remarkable sorbents reported to date revealed how the capability for water uptake of our carbon-GO composite was higher than those reported for PCPs, MOFs and polyoxometalates, and just slightly below that of covalent 2D nanosheets embedded in a polymer matrix. Meanwhile and in terms of preferred uptake, the capability for water versus ethanol uptake of our carbon-GO composite was again higher than those reported for the above-mentioned materials and just

slightly below that of some particular PCPs. Based on this, we could conclude that, in overall terms, our carbon-GO composite indeed exhibited a remarkable performance as compared to other sorbents reported to date. Lower panel in Fig. 7 helped to understand the mechanism governing the preferred uptake of water versus alcohol in our carbon-GO composites. These plots represented the time needed to reach equilibrium in the manifold for each specific gas dose in the isotherm of the different compounds. For the carbon-GO composite obtained at 800 °C, this time (in average) was ca. 1600 s for water, whereas it was above 10000 s for both alcohols, thus revealing the kinetic restrictions that methanol and ethanol experienced for adsorption in our carbon-GO composite.

Conclusions

We have described the preparation of porous carbon-GO composites using a chemical synthetic process based on the use of eutectic mixtures. The use of eutectics was by no means trivial since it allowed the homogeneous dispersion of GO flakes in the liquid containing the carbon precursor. Thus, after polymerization and a subsequent carbonization process, we were able to obtain porous carbon-GO composites. The incorporation of GO flakes throughout the carbon structure provided some hydrophilic features to the porous surface that, ultimately, opened the path to water adsorption – e.g., with water uptakes of up to 12 mmol g^{-1} for the carbon-GO composite obtained at 950 °C. Moreover, the porous structure of carbon-GO composites was narrow enough to discriminate water – i.e., with a kinetic diameter of 0.27 nm – from both methanol and ethanol – i.e., with kinetic diameters of 0.38 and 0.45 nm, respectively. In this regard, the carbon-GO composite obtained at 800 °C was particularly effective in the preferential adsorption of water, with water uptakes in the range of low partial pressures more than 25 times greater than those of both methanol and ethanol. The combination of high water uptakes and preferential adsorption of water versus methanol and ethanol found in our carbon-GO composites may make the application of these materials particularly interesting in processes of bioethanol dehydration.

Acknowledgements

This work was supported by MINECO/FEDER (Project Numbers MAT2015-68639-R, MAT2016-80285-P and RTI2018-097728-B-I00). L. Z. Guan acknowledges Chinese Scholarship Council for a PhD research fellowship (CSC NO. 201608330266). C. Cuadrado-Collados acknowledges UA for a research contract. The authors acknowledge P. Carrero for helpful assistance with TGA measurements and M. J. de la Mata and V. Rubio (from Servicio

Interdepartamental de Investigación-SIdI of the Universidad Autónoma de Madrid-UAM) for helpful assistance with DSC measurements.

References

(1). Sevilla, M.; Fuertes, A. B. Chemical and structural properties of carbonaceous products obtained by hydrothermal carbonization of saccharides. *Chem. Eur. J.* **2009,** *15*, 4195-4203.
(2). Liang, C.; Hong, K.; Guiochon, G. A.; Mays, J. W.; Dai, S. Synthesis of a large-scale highly ordered porous carbon film by self-assembly of block copolymers. *Angew. Chem. Int. Ed.* **2004,** *43*, 5785-5789.
(3). Hu, B.; Wang, K.; Wu, L.; Yu, S. H.; Antonietti, M.; Titirici, M. M. Engineering carbon materials from the hydrothermal carbonization process of biomass. *Adv. Mater.* **2010,** *22*, 813-828.
(4). Worsley, M. A.; Satcher Jr, J. H.; Baumann, T. F. Synthesis and characterization of monolithic carbon aerogel nanocomposites containing double-walled carbon nanotubes. *Langmuir* **2008,** *24*, 9763-9766.
(5). Tao, Y.; Noguchi, D.; Yang, C.-M.; Kanoh, H.; Tanaka, H.; Yudasaka, M.; Iijima, S.; Kaneko, K. Conductive and mesoporous single-wall carbon nanohorn/organic aerogel composites. *Langmuir* **2007,** *23*, 9155-9157.
(6). Worsley, M. A.; Pauzauskie, P. J.; Olson, T. Y.; Biener, J.; Satcher Jr, J. H.; Baumann, T. F. Synthesis of graphene aerogel with high electrical conductivity. *J. Am. Chem. Soc.* **2010,** *132*, 14067-14069.
(7). Gutiérrez, M. C.; Carriazo, D.; Ania, C. O.; Parra, J. B.; Ferrer, M. L.; del Monte, F. Deep eutectic solvents as both precursors and structure directing agents in the synthesis of nitrogen doped hierarchical carbons highly suitable for CO_2 capture. *Energy Environ. Sci.* **2011,** *4*, 3535-3544.
(8). Patino, J.; Gutiérrez, M. C.; Carriazo, D.; Ania, C. O.; Parra, J. B.; Ferrer, M. L.; del Monte, F. Deep eutectic assisted synthesis of carbon adsorbents highly suitable for low-pressure separation of CO_2–CH_4 gas mixtures. *Energy Environ. Sci.* **2012,** *5*, 8699-8707.
(9). Patiño, J.; Gutiérrez, M. C.; Carriazo, D.; Ania, C.; Fierro, J.; Ferrer, M. L.; Del Monte, F. DES assisted synthesis of hierarchical nitrogen-doped carbon molecular sieves for selective CO_2 versus N_2 adsorption. *J. Mater. Chem. A* **2014,** *2*, 8719-8729.
(10). Sevilla, M.; Valle-Vigón, P.; Fuertes, A. B. N-doped polypyrrole-based porous carbons for CO_2 capture. *Adv. Funct. Mater.* **2011,** *21*, 2781-2787.
(11). Titirici, M.-M.; White, R. J.; Falco, C.; Sevilla, M. Black perspectives for a green future: hydrothermal carbons for environment protection and energy storage. *Energy Environ. Sci.* **2012,** *5*, 6796-6822.
(12). Bradley, R.; Rand, B. A comparison of the adsorption behaviour of nitrogen, alcohols and water towards active carbons. *Carbon* **1991,** *29*, 1165-1172.
(13). Mowla, D.; Do, D.; Kaneko, K. Adsorption of water vapor on activated carbon: a brief overview. *Chemistry and physics of carbon* **2003,** *28*, 229-229.
(14). Salame, I. I.; Bandosz, T. J. Adsorption of water and methanol on micro-and mesoporous wood-based activated carbons. *Langmuir* **2000,** *16*, 5435-5440.
(15). Furukawa, H.; Gándara, F.; Zhang, Y.-B.; Jiang, J.; Queen, W. L.; Hudson, M. R.; Yaghi, O. M. Water adsorption in porous metal–organic frameworks and related materials. *J. Am. Chem. Soc.* **2014,** *136*, 4369-4381.
(16). Silvestre-Albero, A.; Silvestre-Albero, J.; Sepúlveda-Escribano, A.; Rodríguez-Reinoso, F. Ethanol removal using activated carbon: Effect of porous structure and surface chemistry. *Microporous Mesoporous Mater.* **2009,** *120*, 62-68.

(17). Shigematsu, A.; Yamada, T.; Kitagawa, H. Selective separation of water, methanol, and ethanol by a porous coordination polymer built with a flexible tetrahedral ligand. *J. Am. Chem. Soc.* **2012,** *134*, 13145-13147.
(18). Cao, L. H.; Wei, Y. S.; Xu, H.; Zang, S. Q.; Mak, T. C. Unveiling the Mechanism of Water-Triggered Diplex Transformation and Correlating the Changes in Structures and Separation Properties. *Adv. Funct. Mater.* **2015,** *25*, 6448-6457.
(19). Gupta, A. K.; Nagarkar, S. S.; Boomishankar, R. Zn (ii) coordination polymer of an in situ generated 4-pyridyl (^{4}Py) attached bis (amido) phosphate ligand,$[PO_2(NH_4Py)_2]^-$ showing preferential water uptake over aliphatic alcohols. *Dalton Trans.* **2013,** *42*, 10964-10970.
(20). Sha, Y.; Bai, S.; Lou, J.; Wu, D.; Liu, B.; Ling, Y. Tuning the adsorption behaviors of water, methanol, and ethanol in a porous material by varying the flexibility of substituted groups. *Dalton Trans.* **2016,** *45*, 7235-7239.
(21). Zhang, Y.-J.; Chen, C.; Cai, L.-X.; Tan, B.; Yang, X.-D.; Zhang, J.; Ji, M. Post-cycloaddition modification of a porous MOF for improved GC separation of ethanol and water. *Dalton Trans.* **2017,** *46*, 7092-7097.
(22). Plessius, R.; Kromhout, R.; Ramos, A. L. D.; Ferbinteanu, M.; Mittelmeijer-Hazeleger, M. C.; Krishna, R.; Rothenberg, G.; Tanase, S. Highly Selective Water Adsorption in a Lanthanum Metal–Organic Framework. *Chem. Eur. J.* **2014,** *20*, 7922-7925.
(23). Sadakiyo, M.; Yamada, T.; Kato, K.; Takata, M.; Kitagawa, H. A significant change in selective adsorption behaviour for ethanol by flexibility control through the type of central metals in a metal–organic framework. *Chem. Sci.* **2016,** *7*, 1349-1356.
(24). Hu, J.; Xu, Y.; Zhang, D.; Chen, B.; Lin, Z.; Hu, C. A Highly Symmetric Ionic Crystal Constructed by Polyoxoniobates and Cobalt Complexes for Preferential Water Uptake over Alcohols. *Inorg. Chem.* **2017,** *56*, 10844-10847.
(25). Yeh, T.-M.; Wang, Z.; Mahajan, D.; Hsiao, B. S.; Chu, B. High flux ethanol dehydration using nanofibrous membranes containing graphene oxide barrier layers. *J. Mater. Chem. A* **2013,** *1*, 12998-13003.
(26). Nair, R.; Wu, H.; Jayaram, P.; Grigorieva, I.; Geim, A. Unimpeded permeation of water through helium-leak–tight graphene-based membranes. *Science* **2012,** *335*, 442-444.
(27). Sakamoto, H.; Fujimori, T.; Li, X.; Kaneko, K.; Kan, K.; Ozaki, N.; Hijikata, Y.; Irle, S.; Itami, K. Cycloparaphenylene as a molecular porous carbon solid with uniform pores exhibiting adsorption-induced softness. *Chem. Sci.* **2016,** *7*, 4204-4210.
(28). Marsh, H.; Reinoso, F. R., *Activated carbon*. Elsevier: 2006.
(29). Carriazo, D.; Serrano, M. C.; Gutiérrez, M. C.; Ferrer, M. L.; del Monte, F. Deep-eutectic solvents playing multiple roles in the synthesis of polymers and related materials. *Chem. Soc. Rev.* **2012,** *41*, 4996-5014.
(30). Abbott, A. P.; Capper, G.; Davies, D. L.; Rasheed, R. K.; Tambyrajah, V. Novel solvent properties of choline chloride/urea mixtures. *Chem. Commun.* **2003**, 70-71.
(31). Abbott, A. P.; Harris, R. C.; Ryder, K. S. Application of hole theory to define ionic liquids by their transport properties. *J. Phys. Chem. B* **2007,** *111*, 4910-4913.
(32). Abbott, A. P.; Capper, G.; Gray, S. Design of improved deep eutectic solvents using hole theory. *ChemPhysChem* **2006,** *7*, 803-806.
(33). Abbott, A. P.; Boothby, D.; Capper, G.; Davies, D. L.; Rasheed, R. K. Deep eutectic solvents formed between choline chloride and carboxylic acids: versatile alternatives to ionic liquids. *J. Am. Chem. Soc.* **2004,** *126*, 9142-9147.
(34). Francisco, M.; van den Bruinhorst, A.; Kroon, M. C. Low-transition-temperature mixtures (LTTMs): A new generation of designer solvents. *Angew. Chem. Int. Ed.* **2013,** *52*, 3074-3085.
(35). Carriazo, D.; Gutiérrez, M. a. C.; Ferrer, M. L.; del Monte, F. Resorcinol-based deep eutectic solvents as both carbonaceous precursors and templating agents in the synthesis of hierarchical porous carbon monoliths. *Chem. Mater.* **2010,** *22*, 6146-6152.

(36). del Monte, F.; Carriazo, D.; Serrano, M. C.; Gutiérrez, M. C.; Ferrer, M. L. Deep eutectic solvents in polymerizations: a greener alternative to conventional syntheses. *ChemSusChem* **2014,** *7*, 999-1009.
(37). Carriazo, D.; Gutiérrez, M. C.; Picó, F.; Rojo, J. M.; Fierro, J. L.; Ferrer, M. L.; del Monte, F. Phosphate-Functionalized Carbon Monoliths from Deep Eutectic Solvents and their Use as Monolithic Electrodes in Supercapacitors. *ChemSusChem* **2012,** *5*, 1405-1409.
(38). Carriazo, D.; Gutiérrez, M. C.; Jiménez, R.; Ferrer, M. L.; del Monte, F. Deep-Eutectic-Assisted Synthesis of Bimodal Porous Carbon Monoliths with High Electrical Conductivities. *Particle & Particle Systems Characterization* **2013,** *30*, 316-320.
(39). López-Salas, N.; del Monte, F.; Tamayo, A.; Fierro, J. L. G.; De Lacey, A. L.; Ferrer, M. L.; Gutiérrez, M. C. Sulfur-Doped Carbons Prepared from Eutectic Mixtures Containing Hydroxymethylthiophene as Metal-Free Oxygen Reduction Catalysts. *ChemSusChem* **2014,** *7*, 3347-3355.
(40). López-Salas, N.; Gutierrez, M. C.; Ania, C. O.; Fierro, J. L. G.; Ferrer, M. L.; del Monte, F. Efficient nitrogen-doping and structural control of hierarchical carbons using unconventional precursors in the form of deep eutectic solvents. *J. Mater. Chem. A* **2014,** *2*, 17387-17399.
(41). López-Salas, N.; Gutiérrez, M. C.; Ania, C. O.; Muñoz-Márquez, M. A.; Ferrer, M. L.; del Monte, F. Nitrogen-doped carbons prepared from eutectic mixtures as metal-free oxygen reduction catalysts. *J. Mater. Chem. A* **2015,** *4*, 478-488.
(42). López-Salas, N.; Carriazo, D.; Gutiérrez, M.; Ferrer, M. L.; Ania, C.; Rubio, F.; Tamayo, A.; Fierro, J. L. G.; del Monte, F. Tailoring the textural properties of hierarchical porous carbons using deep eutectic solvents. *J. Mater. Chem. A* **2016,** *4*, 9146-9159.
(43). Gutiérrez, M. C.; Carriazo, D.; Tamayo, A.; Jiménez, R.; Picó, F.; Rojo, J. M.; Ferrer, M. L.; del Monte, F. Deep-Eutectic-Solvent-Assisted Synthesis of Hierarchical Carbon Electrodes Exhibiting Capacitance Retention at High Current Densities. *Chem. Eur. J.* **2011,** *17*, 10533-10537.
(44). Patiño, J.; López-Salas, N.; Gutiérrez, M. C.; Carriazo, D.; Ferrer, M. L.; del Monte, F. Phosphorus-doped carbon–carbon nanotube hierarchical monoliths as true three-dimensional electrodes in supercapacitor cells. *J. Mater. Chem. A* **2016,** *4*, 1251-1263.
(45). Hummers Jr, W. S.; Offeman, R. E. Preparation of graphitic oxide. *J. Am. Chem. Soc.* **1958,** *80*, 1339-1339.
(46). Carriazo, D.; Patiño, J.; Gutiérrez, M. C.; Ferrer, M. L.; del Monte, F. Microwave-assisted synthesis of $NiCo_2O_4$–graphene oxide nanocomposites suitable as electrodes for supercapacitors. *RSC Advances* **2013,** *3*, 13690-13695.
(47). López-Salas, N.; Jardim, E. O.; Silvestre-Albero, A.; Gutiérrez, M. C.; Ferrer, M. L.; Rodríguez-Reinoso, F.; Silvestre-Albero, J.; Del Monte, F. Use of eutectic mixtures for preparation of monolithic carbons with CO_2-adsorption and gas-separation capabilities. *Langmuir* **2014,** *30*, 12220-12228.
(48). Silvestre-Albero, J.; De Salazar, C. G.; Sepúlveda-Escribano, A.; Rodrıguez-Reinoso, F. Characterization of microporous solids by immersion calorimetry. *Colloids Surf. A* **2001,** *187*, 151-165.
(49). Roldán-Ruiz, M.; Jiménez-Riobóo, R.; Gutiérrez, M.; Ferrer, M.; del Monte, F. Brillouin and NMR spectroscopic studies of aqueous dilutions of malicine: Determining the dilution range for transition from a “water-in-DES” system to a “DES-in-water” one. *J. Mol. Liq.* **2019**.
(50). Gutiérrez, M. a. C.; Ferrer, M. a. L.; Mateo, C. R.; del Monte, F. Freeze-drying of aqueous solutions of deep eutectic solvents: a suitable approach to deep eutectic suspensions of self-assembled structures. *Langmuir* **2009,** *25*, 5509-5515.
(51). Gutiérrez, M. a. C.; Rubio, F.; Del Monte, F. Resorcinol-formaldehyde polycondensation in deep eutectic solvents for the preparation of carbons and carbon− carbon nanotube composites. *Chem. Mater.* **2010,** *22*, 2711-2719.
(52). Gutiérrez, M. C.; Ferrer, M. L.; Yuste, L.; Rojo, F.; del Monte, F. Bacteria incorporation in deep-eutectic solvents through freeze-drying. *Angew. Chem.Int.Ed.* **2010,** *122*, 2204-2208.

(53). Akhavan, O.; Ghaderi, E.; Esfandiar, A. Wrapping bacteria by graphene nanosheets for isolation from environment, reactivation by sonication, and inactivation by near-infrared irradiation. *J. Phys. Chem. B* **2011,** *115*, 6279-6288.
(54). Akhavan, O.; Ghaderi, E. Escherichia coli bacteria reduce graphene oxide to bactericidal graphene in a self-limiting manner. *Carbon* **2012,** *50*, 1853-1860.
(55). Feng, H.; Cheng, R.; Zhao, X.; Duan, X.; Li, J. A low-temperature method to produce highly reduced graphene oxide. *Nat. Commun.* **2013,** *4*, 1539.
(56). Guan, L. Z.; Gutiérrez, M. C.; Yuste, L.; Rojo, F.; Ferrer, M. L.; del Monte, F. Vortex ring processes allowing shape control and entrapment of antibacterial agents in GO-based particles. *Carbon* **2019**.
(57). Krishnamoorthy, K.; Veerapandian, M.; Yun, K.; Kim, S.-J. The chemical and structural analysis of graphene oxide with different degrees of oxidation. *Carbon* **2013,** *53*, 38-49.
(58). Zhang, X.; Solomon, D. H. The reaction of furfuryl alcohol resins with hexamethylenetetramine: A 13C and 15N high-resolution solid-state NMR study. *J. Polym. Sci. B* **1997,** *35*, 2233-2243.
(59). Kim, N. H.; Kuila, T.; Lee, J. H. Simultaneous reduction, functionalization and stitching of graphene oxide with ethylenediamine for composites application. *J. Mater. Chem. A* **2013,** *1*, 1349-1358.
(60). Wang, G.; Yang, J.; Park, J.; Gou, X.; Wang, B.; Liu, H.; Yao, J. Facile synthesis and characterization of graphene nanosheets. *J. Phys. Chem. C* **2008,** *112*, 8192-8195.
(61). Estrade-Szwarckopf, H. XPS photoemission in carbonaceous materials: A "defect" peak beside the graphitic asymmetric peak. *Carbon* **2004,** *42*, 1713-1721.
(62). Ros, T. G.; Van Dillen, A. J.; Geus, J. W.; Koningsberger, D. C. Surface oxidation of carbon nanofibres. *Chem. Eur. J.* **2002,** *8*, 1151-1162.
(63). Xie, Y.; Sherwood, P. M. X-ray photoelectron spectroscopic studies of carbon fiber surfaces. Part 10. Valence-band studies interpreted by X-. alpha. calculations and the differences between PAN-and pitch-based fibers. *Chem. Mater.* **1989,** *1*, 427-432.
(64). Kapteijn, F.; Moulijn, J.; Matzner, S.; Boehm, H.-P. The development of nitrogen functionality in model chars during gasification in CO_2 and O_2. *Carbon* **1999,** *37*, 1143-1150.
(65). Pels, J.; Kapteijn, F.; Moulijn, J.; Zhu, Q.; Thomas, K. Evolution of nitrogen functionalities in carbonaceous materials during pyrolysis. *Carbon* **1995,** *33*, 1641-1653.
(66). Liu, L.; Yang, J.; Li, J.; Dong, J.; Šišak, D.; Luzzatto, M.; McCusker, L. Ionothermal Synthesis and Structure Analysis of an Open-Framework Zirconium Phosphate with a High CO2/CH4 Adsorption Ratio. *Angew. Chem.Int.Ed.* **2011,** *123*, 8289-8292.
(67). Jeon, Y. M.; Armatas, G. S.; Heo, J.; Kanatzidis, M. G.; Mirkin, C. A. Amorphous infinite coordination polymer microparticles: a new class of selective hydrogen storage materials. *Adv. Mater.* **2008,** *20*, 2105-2110.
(68). López-Salas, N.; Ferrer, M.; Gutiérrez, M.; Fierro, J.; Cuadrado-Collados, C.; Gandara-Loe, J.; Silvestre-Albero, J.; del Monte, F. Hydrogen-bond supramolecular hydrogels as efficient precursors in the preparation of freestanding 3D carbonaceous architectures containing BCNO nanocrystals and exhibiting a high CO_2/CH_4 adsorption ratio. *Carbon* **2018,** *134*, 470-479.
(69). Wahby, A.; Silvestre-Albero, J.; Sepúlveda-Escribano, A.; Rodríguez-Reinoso, F. CO_2 adsorption on carbon molecular sieves. *Microporous Mesoporous Mater.* **2012,** *164*, 280-287.
(70). López-Salas, N.; Jardim, E. O.; Silvestre-Albero, A.; Gutiérrez, M.; Ferrer, M.; Rodríguez-Reinoso, F.; Silvestre-Albero, J.; Del Monte, F. Use of eutectic mixtures for preparation of monolithic carbons with CO_2-adsorption and gas-separation capabilities. *Langmuir* **2014,** *30*, 12220-12228.
(71). Yang, H.; Wu, H.; Xu, Z.; Mu, B.; Lin, Z.; Cheng, X.; Liu, G.; Pan, F.; Cao, X.; Jiang, Z. Hierarchical pore architectures from 2D covalent organic nanosheets for efficient water/alcohol separation. *J. Membr. Sci.* **2018,** *561*, 79-88.
(72). Yang, H.; Wu, H.; Yao, Z.; Shi, B.; Xu, Z.; Cheng, X.; Pan, F.; Liu, G.; Jiang, Z.; Cao, X. Functionally graded membranes from nanoporous covalent organic frameworks for highly selective water permeation. *J. Mater. Chem. A* **2018,** *6*, 583-591.

(73). Darvishi, M.; Foroutan, M. Mechanism of water separation from a gaseous mixture via nanoporous graphene using molecular dynamics simulation. *RSC Advances* **2015,** *5*, 81282-81294.
(74). Ying, Y.; Liu, D.; Zhang, W.; Ma, J.; Huang, H.; Yang, Q.; Zhong, C. High-Flux Graphene Oxide Membranes Intercalated by Metal–Organic Framework with Highly Selective Separation of Aqueous Organic Solution. *ACS Appl. Mater. Interfaces* **2017,** *9*, 1710-1718.
(75). Liu, L.; Tan, S. J.; Horikawa, T.; Do, D. D.; Nicholson, D.; Liu, J. Water adsorption on carbon - A review. *Adv. Colloid Interface Sci.* **2017,** *250*, 64-78.
(76). Fletcher, A. J.; Uygur, Y.; Thomas, K. M. Role of Surface Functional Groups in the Adsorption Kinetics of Water Vapor on Microporous Activated Carbons. *J. Phys. Chem. C* **2007,** *111*, 8349-8359.
(77). Bourrelly, S.; Moulin, B.; Rivera, A.; Maurin, G.; Devautour-Vinot, S.; Serre, C.; Devic, T.; Horcajada, P.; Vimont, A.; Clet, G.; Daturi, M.; Lavalley, J.-C.; Loera-Serna, S.; Denoyel, R.; Llewellyn, P. L.; Férey, G. Explanation of the Adsorption of Polar Vapors in the Highly Flexible Metal Organic Framework MIL-53(Cr). *J. Am. Chem. Soc.* **2010,** *132*, 9488-9498.

Figure 1: DSC scan taken at a rate of 5 °C/min of the mixture of PA, EA and Gly in a 1:2:1 molar ratio – e.g., $PAEAGly_{DES}$ – right after preparation (black line), after lyophilisation (red line), and after mixing with GO and lyophilisation (blue line). The water content in $PAEAGly_{DES}$ was 5.5 wt% right after preparation and 1.9 wt% after lyophilisation. The water content in the dispersion of GO in $PAEAGly_{DES}$ was 5.9 wt%. The melting point (T_m) of $PAEAGly_{DES}$ was at ca. 20 °C right after preparation and at ca. 36 °C after lyophilisation. The melting point (T_m) of the dispersion of GO in $PAEAGly_{DES}$ was at ca. 16 °C.

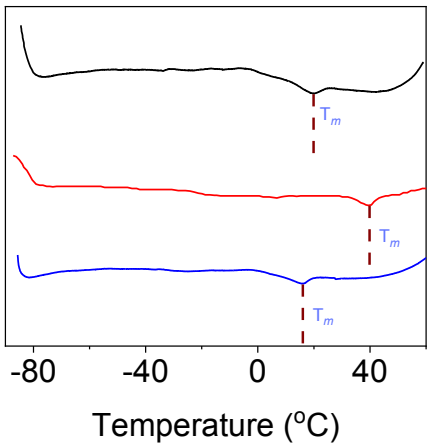

Figure 2: TEM (a, b), XPS (c) and XRD (d) of GO. Bars are 180 nm in (a) and 500 nm in (b).

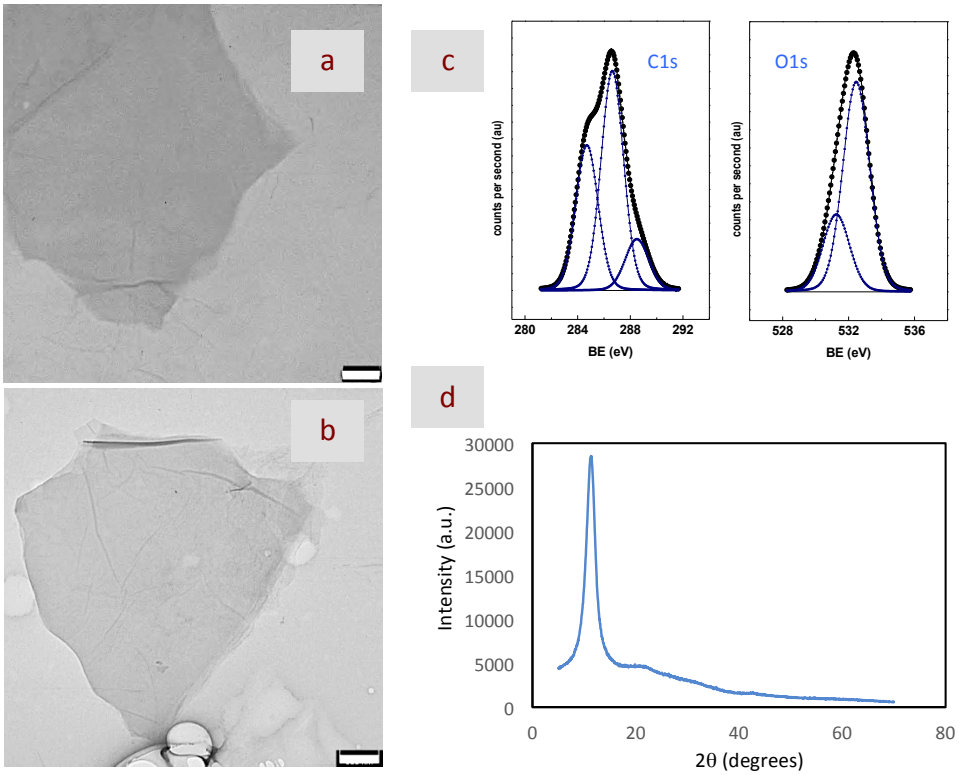

Figure 3: Raman spectra of GO (grey line), GO thermally treated at 800 °C (red line), carbon-GO composites obtained after carbonization at 800 °C (blue line), and the same carbon obtained after carbonization at 800 °C but without GO (green line).

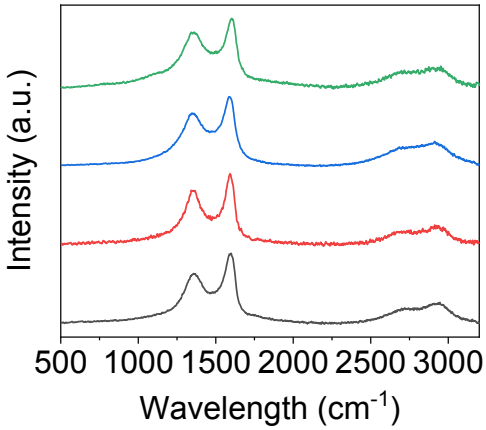

Figure 4: Picture of (a) a GO suspension in $PAEAGly_{DES}$ and (b) a carbon-GO composite obtained after carbonization at 800 °C in monolithic form under a mass of 100 g. A Young modulus of 1145 MPa and a phase angle of 3.5 ° were obtained from triple-point bending tests carried out on a carbon-GO composite in the form of monolithic cylinder and with the axis of the cylinder aligned parallel to the applied force.

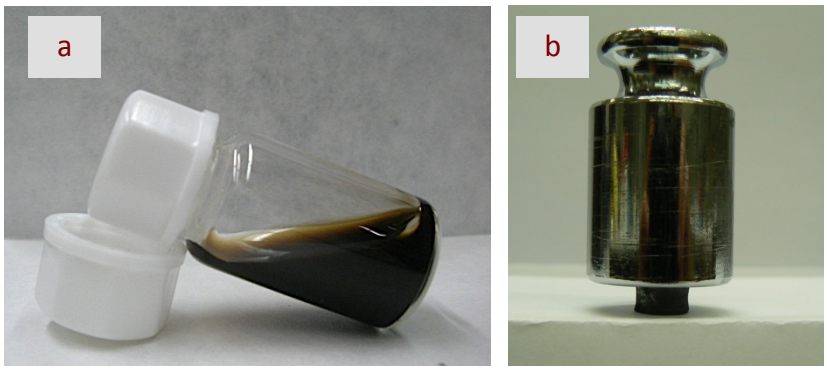

Figure 5: FTIR (a) and solid state ^{13}C CPMAS NMR (b) of the FA polymer obtained after polycondensation.

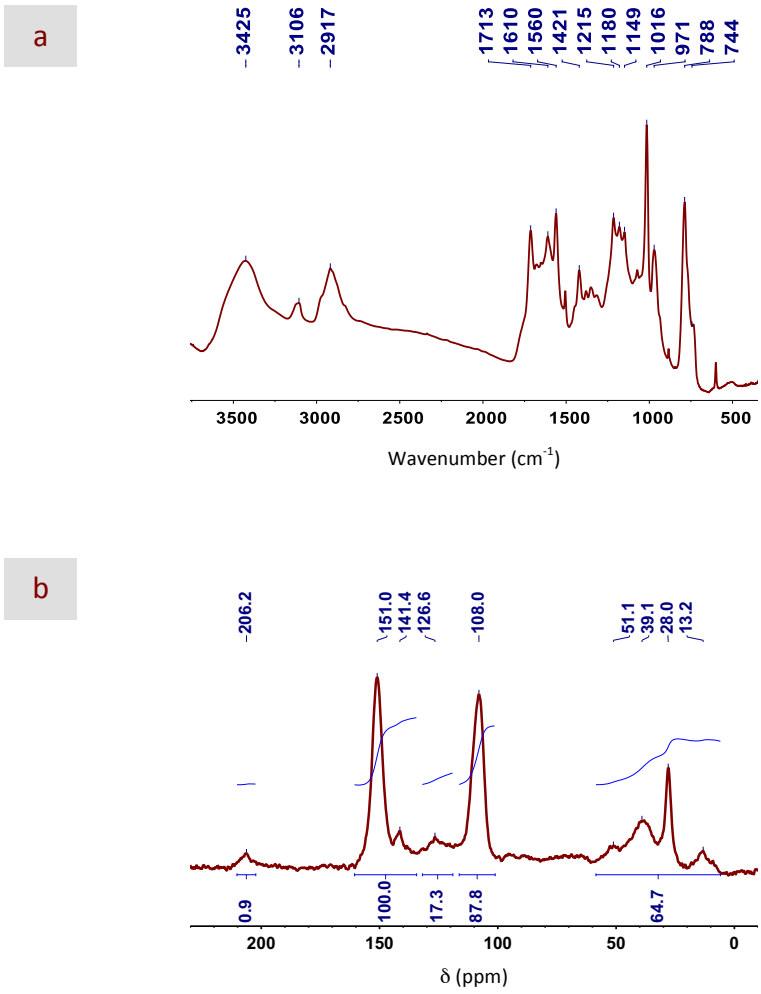

Figure 6: SEM (a, b) and TEM (c) micrographs, XRD pattern (d), ^{31}P NMR spectrum (e), and XPS spectra (f) of carbon-GO composites obtained after carbonization at 800 °C. Bars are 100 μm in (a), 10 μm in (b), and 360 nm in (c).

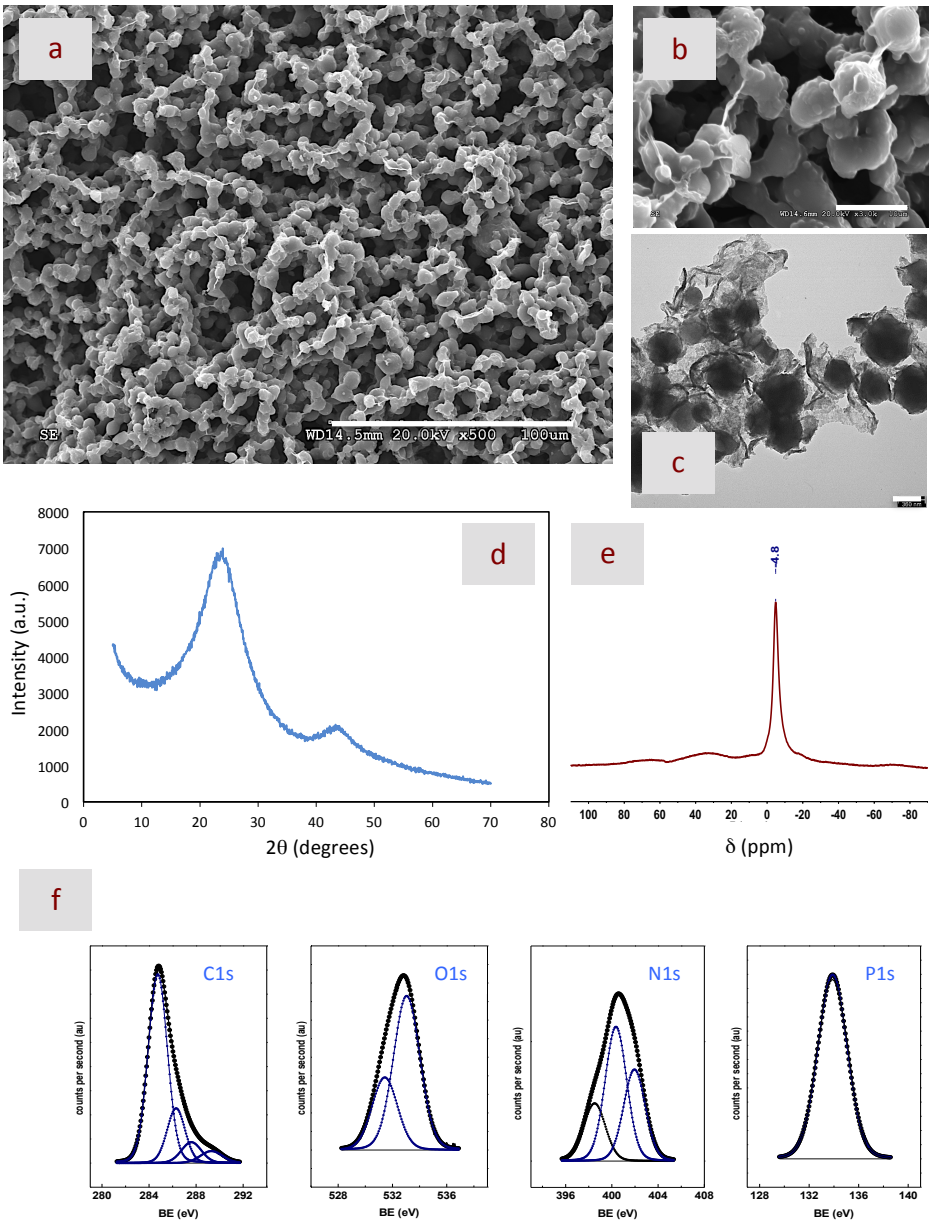

Table 1: Comparison of water, methanol and ethanol uptakes (at 298 K) obtained for some of the most suitable materials reported to date for alcohol dehydration and for the carbon-GO composites obtained in this work after carbonization at 800 and 950 °C. Data are provided in mmol/g (top) and cm^3/g (bottom).

Reference	Water uptake (mmol/g)	Methanol uptake (mmol/g)	Ethanol uptake (mmol/g)	Water uptake vs. Methanol uptake	Water uptake vs. Ethanol uptake
This work[a]	3.1[g]/9.7[h]	0.12[g]/3.7[h]	0.1[g]/1.3[h]	26[g]/2.6[h]	31[g]/7.5[h]
This work[b]	1.7[g]/12.1[h]	0.2[g]/4.9[h]	0.1[g]/2.0[h]	8.5[g]/2.5[h]	17[g]/6[h]
17[c]	0.7[g]/1.7[h]	0.12[g]/1.72[h]	0.03[g]/0.17[h]	5.7[g]/1[h]	20[g]/10[h]
20[d]	1.3[g]/3.6[i]	3.6[g]/4.0[i]	0.1[g]/2.5[i]	0.4[g]/0.9[i]	13[g]/1.4[i]
21[d]	0.03[g]/2.9[j]	0.90[g]/3.2[j]	0.01[g]/0.21[j]	0.03[g]/0.90[j]	3[g]/13.8[j]
22[d]	0.17[g]/1.1[h]	0.02[g]/0.05[h]	--	8.5[g]/21.6[h]	--
24[e]	0.1[g]/5.0[i]	1.3[g]/2.2[i]	0.6[g]/1.2[i]	0.08[g]/2.3[i]	0.2[g]/4.2[i]
71[f]	2.1[g]/24.1[i]	--	0.4[g]/8.0[i]	--	4.7[g]/3[i]

Reference	Water uptake (cm^3/g)	Methanol uptake (cm^3/g)	Ethanol uptake (cm^3/g)	Water uptake vs. Methanol uptake	Water uptake vs. Ethanol uptake
This work[a]	0.060[g]/0.175[h]	0.005[g]/0.149[h]	0.006[g]/0.076[h]	11.5[g]/1.2[h]	9.55[g]/2.3[h]
This work[b]	0.030[g]/0.220[h]	0.008[g]/0.198[h]	0.006[g]/0.117[h]	3.8[g]/1.1[h]	5.2[g]/1.9[h]
17[c]	0.012[g]/0.031[h]	0.005[g]/0.069[h]	0.002[g]/0.010[h]	2.6[g]/0.44[h]	7.1[g]/3.1[h]
20[d]	0.023[g]/0.065[i]	0.146[g]/0.162[i]	0.006[g]/0.146[i]	0.2[g]/0.4[i]	4.0[g]/0.4[i]
21[d]	0.0005[g]/0.052[j]	0.036[g]/0.129[j]	0.001[g]/0.012[j]	0.01[g]/0.4[j]	0.9[g]/4.3[j]
22[d]	0.003[g]/0.019[h]	0.001[g]/0.002[h]	--	3.8[g]/9.6[h]	--
24[e]	0.002[g]/0.090[i]	0.053[g]/0.089[i]	0.035[g]/0.070[i]	0.03[g]/1.0[i]	0.05[g]/1.3[i]
71[f]	0.038[g]/0.434[i]	--	0.023[g]/0.467[i]	--	1.6[g]/0.9[i]

[a] Carbon-GO composite carbonized at 800 °C; [b] Carbon-GO composite carbonized at 950 °C; [c] Porous coordination polymer; [d] MOF; [e] Polyoxometalate; [f] Covalent nanosheets in polymer; [g] At $P/P_0 = 0.1$; [h] At $P/P_0 = 0.99$; [i] At $P/P_0 = 0.9$; [j] At $P/P_0 = 0.85$

Figure 7: Upper panel - Water, methanol and ethanol vapour adsorption isotherms (at 298 K) of carbon-GO composites obtained after carbonization at 800 °C. Lower panel - Equilibrium time (time required for the manifold pressure to reach equilibrium) for each specific vapor dose is also included for the three probe molecules.

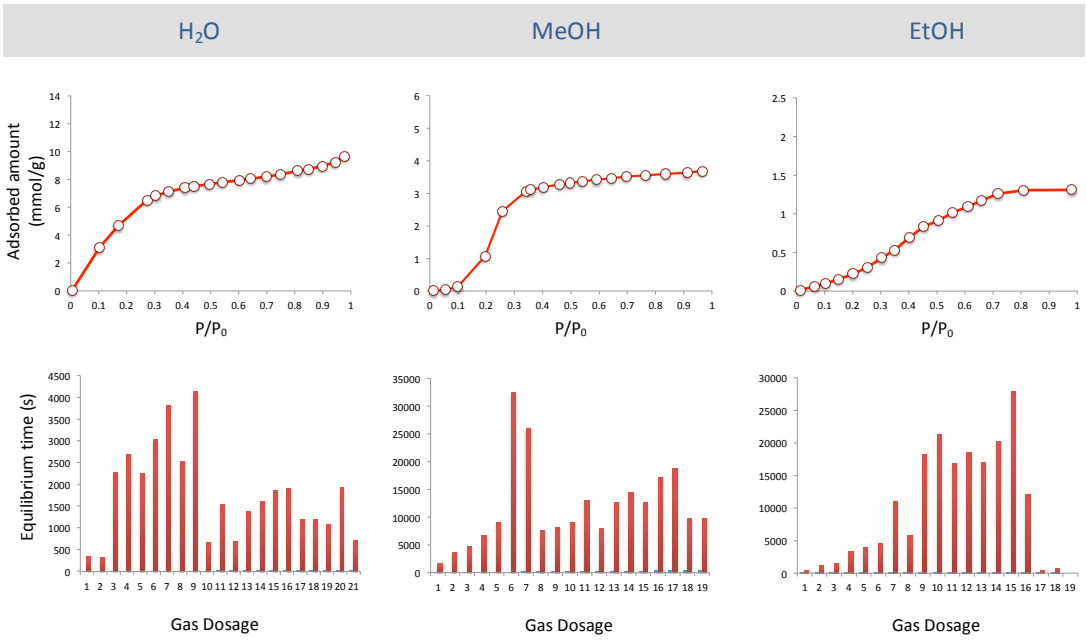

TOC graphic

Carbon-GO composite with high H_2O/MeOH and H_2O/EtOH adsorption ratios